International Journal of Multiphase Flow 36 (2010) 491–502

Contents lists available at ScienceDirect

International Journal of Multiphase Flow

journal homepage: www.elsevier.com/locate/ijmulflow

Dynamic pressure based prediction of spray cooling heat transfer coefficients

Bahman Abbasi [a], Jungho Kim [a,*], Andre Marshall [b]

[a] Dept. of Mechanical Engineering, University of Maryland, College Park, MD 20742, USA
[b] Dept. of Fire Protection Engineering, University of Maryland, College Park, MD 20742, USA

ARTICLE INFO

Article history:
Received 25 September 2009
Received in revised form 20 January 2010
Accepted 27 January 2010
Available online 8 February 2010

Keywords:
Spray cooling
Heat transfer
Single-phase
Correlation

ABSTRACT

An important goal of spray cooling research is the ability to predict local heat transfer from the spray hydrodynamics. It is postulated that the local normal pressure exerted by the spray onto the heated surface can be used to obtain the local heat transfer coefficient. This hypothesis was tested using data obtained from hollow cone, full cone, and linear sprays at four nozzle pressures and three stand-off distances. A correlation between the pressure and heat transfer coefficient was determined from the data, then used to "predict" the heat transfer coefficient to verify the accuracy of the correlation. The area averaged heat transfer coefficient could be predicted within 25%, indicating that pressure can be used to predict the local heat transfer coefficient in the single-phase regime.

1. Introduction

Spray cooling occurs when liquid forced through a small orifice shatters into a dispersion of fine droplets which then impact a heated surface. The droplets spread on the surface and evaporate or form a thin liquid film, removing large amounts of energy at low temperatures due to the latent heat of evaporation in addition to substantial single-phase convection effects. Heat transfer rates much higher than can be attained in pool boiling are possible with sprays since vapor can be removed from the heated surface more easily, allowing liquid to be supplied to the surface more easily (e.g., Chen, 1966). A review of spray cooling heat transfer is given in Kim (2007).

Spray cooling data are generally plotted as heat flux vs. wall temperature. At low wall temperatures, the curves are typically linear, indicating the heat transfer is dominated by single-phase convection, although some evaporation can also occur. Usually, the supply of cold liquid is so high (in order to maximize heat transfer) that there is little time for the surface to significantly heat the liquid, and the liquid is swept away before it can heat up enough to generate a bubble. High wall temperatures are required to begin significant bubble nucleation. Droplet impact onto the liquid film can also provide significant agitation, increasing the amount of heat transferred. Pautsch and Shedd (2006) verified this using a total internal reflection technique to measure the local film thickness produced by sprays. The film thickness was found to be unaffected when a heat flux of 15 W/cm^2 was applied, indicating that the heat transfer mechanism was dominated by single-phase convection instead of evaporation. Heat transfer increases with increasing flow rate for a number of reasons. A larger fluid flow results in higher liquid velocity over the surface and a thinner thermal boundary layer, similar to what occurs in jets. The droplet impact onto the film can also agitate the liquid, thinning the thermal boundary layer locally. As the superheat is increased, phase change becomes important and is indicated by an increase in the slope of the spray cooling curve and the heater begins to dry out outside the droplet impact area. Horacek et al. (2005) found that a progressively larger fraction of the heater dries out as critical heat flux (CHF) is approached.

An important goal of spray cooling research is the ability to predict the local heat transfer coefficient (h), in the single-phase regime for given spray hydrodynamics (droplet size, droplet velocity, droplet number density, etc.), impact angle, and nozzle configuration (nozzle-to-surface distance, nozzle orientation, number of nozzles, etc.). The detailed mechanisms of spray cooling are extremely complicated. A summary of the many ways in which single droplets behave upon impact with a solid surface and thin liquid layers have been summarized by Yarin (2006). Photographs showing single droplet behavior under various conditions (Fig. 1) along with a list of parameters and their effect on the droplet behavior was given by Rioboo et al. (2001). It is evident that mechanistic prediction of single droplet behavior is difficult, and that prediction of millions of droplets of varying diameter striking a

* Corresponding author. Tel.: +1 301 405 5437.
E-mail address: kimjh@umd.edu (J. Kim).

0301-9322/$ - see front matter © 2010 Elsevier Ltd. All rights reserved.
doi:10.1016/j.ijmultiphaseflow.2010.01.007

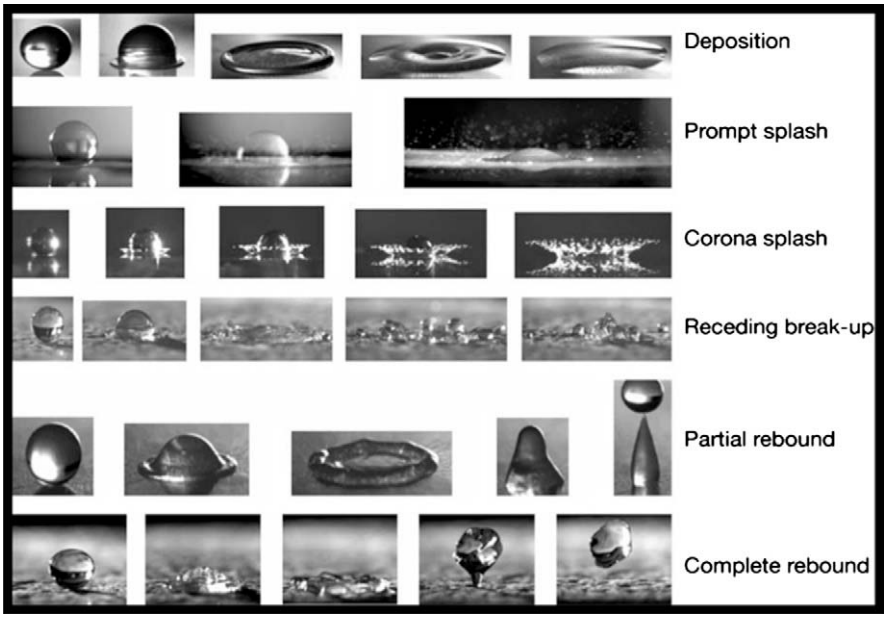

Fig. 1. Summary of droplet behavior upon impact, from Rioboo et al. (2001).

surface with different speeds at various times and interacting with each other will not be possible in the foreseeable future.

There are also little data and/or correlations available from which h can be predicted in the single-phase regime. It has been suggested that local volumetric flux is the controlling parameter in the spray cooling heat transfer. Shedd (2007) assumed that the spray produced a liquid film on the surface that could be described through a two-layer model where a turbulent liquid layer flowed over a thin viscous sublayer of thickness δ_v. The heat transfer coefficient could be expressed as

$$h = \frac{k}{\delta_T} = \frac{k}{\delta_v}\mathrm{Pr}^n \tag{1}$$

where δ_T is the thermal boundary layer thickness. In the sublayer, the non-dimensional velocity profile is $u^+ = y^+$, or $\delta_v = \frac{\beta\nu}{\sqrt{\tau/\rho}}$ where β is a constant. The heat transfer coefficient could then be written

$$h = \beta\frac{k}{\nu}\sqrt{\frac{\tau}{\rho}}\mathrm{Pr}^n \tag{2}$$

Since the shear stress τ was not known, he assumed that it could be related to the volumetric flow rate, $\overline{Q}''$ [m^3/m^2 s], of droplets striking the surface. The final form of his correlation was

$$h = \beta_1 c_p \rho \overline{Q}''^{0.5}\mathrm{Pr}^{-0.5} \tag{3}$$

The value of the constant β_1 depended on the spray system geometry. For single nozzle conical sprays, $\beta_1 = 0.149\ \mathrm{m}^{0.5}\ \mathrm{s}^{-0.5}$, while the four-nozzle arrays were about 14% less efficient, resulting in $\beta_1 = 0.129\ \mathrm{m}^{0.5}\ \mathrm{s}^{-0.5}$. The droplet size and velocity were not assumed to have significant influence on the heat transfer.

Rybicki and Mudawar (2006) suggested the following correlation for PF-5052 and water sprays in the single-phase regime:

$$Nu_{d_{32}} = 4.7\mathrm{Re}_{d_{32}}^{0.61}\mathrm{Pr}_f^{0.32} \tag{4}$$

where $Nu_{d_{32}} = \frac{q''}{T_{surface}-T_{liquid}}\frac{d_{32}}{k} = \frac{hd_{32}}{k}$, $\mathrm{Re} = \frac{\rho\overline{Q}''d_{32}}{\mu}$, $\mathrm{Pr} = \frac{\mu c_p}{k}$, q'' is the heat flux, d_{32} is the Sauter mean diameter, k is the thermal conductivity, ρ is the density, $\overline{Q}''$ is the volumetric flux of liquid onto the surface, μ is the dynamic viscosity, and c_p is the specific heat. They assumed h depended on the volumetric flow rate of droplets onto the surface, and Eq. (4) fit their data with an overall mean absolute error of 13.1%.

Both of the above correlations assume the spray cooling heat transfer depends primarily on the local volumetric flux. For simplicity, consider a spray containing droplets of uniform diameter (d). The volumetric flux is given by

$$\overline{Q}'' = \frac{\pi d^3}{6}NV \tag{5}$$

where N is the droplet number concentration and V is the droplet velocity. Shedd's correlation (Eq. (3)) suggests that the heat transfer coefficient remains constant if $\overline{Q}''$ remains constant, irrespective of large variations in d, V, and N. Similarly, the Rybicki and Mudawar correlation (Eq. (4)) yields constant heat transfer coefficient if the quantity $\frac{\overline{Q}''^{0.61}}{d_{32}^{0.39}} \propto N^{0.61}d_{32}^{1.44}V^{0.61}$ remains constant.

It is the thesis of the current paper is that the spray heat transfer depends primarily on the *kinetic energy* of the incoming droplets rather than just the flow rate of liquid through the nozzle. The droplets transfer this energy to the liquid film in the form of local boundary layer thinning and increased agitation, the amount of which is related to the dynamic pressure exerted by the droplets onto the surface. This connection is also suggested by studies of droplets striking free liquid surfaces. For example, Prosperetti and Oguz (1993) showed that the depth to which a liquid mass penetrated a deep pool of liquid depended on its initial kinetic energy at impact. They used the Froude number and Weber number (both representing the droplet kinetic energy) to predict the radius of a hemispherical cavity in the liquid layer created by droplet impingement. Zhu et al. (2000) and Fedorchenko and Wang (2004) also used the droplet kinetic energy described in terms of the Weber and Froude number to estimate the droplet penetration length. A similar approach has been implemented in numerical studies such as those of Weiss and Yarin (1999) and Josserand and Zaleski (2003), where different combinations of Froude, Weber, and Reynolds numbers were used to study droplet impact on films. These studies indicate that the kinetic energy of the droplets (manifested in this paper in form of the impingement pressure), and not the mass flux, is widely regarded as important in describ-

ing the droplet impact phenomena. It is expected to be just as important in heat transfer.

An experimentally verified correlation between the local pressure and the heat transfer coefficient would allow the local heat transfer to be predicted from the easily measured pressure distributions produced by single nozzles as well as multiple overlapping nozzles over a wide range of operating conditions. The expected form of the relation between the pressure and heat transfer coefficient can be obtained from dimensional analysis. Assume the local heat transfer coefficient is dependent on the local pressure and fluid properties:

$$h = f(P, \mu, \rho, c_p, k) \tag{6}$$

Non-dimensionalizing yields

$$H = \frac{h}{(\rho P)^{1/2} c_p} = C\mathrm{Pr}^a \tag{7}$$

where H is a non-dimensional heat transfer coefficient, and C and a are constants that need to be determined from experiment. H is similar to the Stanton number $\left(St = \frac{h}{\rho u_\infty c_p}\right)$ used in boundary layer theory, but with h normalized by the normal pressure instead of the freestream velocity. The relation between h and P is then given by

$$h = C_1 P^{1/2} \tag{8}$$

where $C_1 = C\rho^{1/2} c_p \mathrm{Pr}^a$ is a constant that depends on fluid properties. To test this hypothesis, local pressure and heat transfer coefficient data were collected for hollow cone, full cone, and flat fan sprays and compared with the pressure-heat transfer correlation given in Eq. (8). A description of the experimental apparatus along with a discussion of the results is given below.

2. Experimental apparatus

Three test rigs were designed and constructed to measure the spray characteristics, the local pressure, and the local heat transfer. The working fluid was PF-5060 (T_{sat} = 56 °C at 1 atm). A brief description of each follows.

2.1. Spray characteristics

Three spray nozzles were used to produce different sprays: hollow cone spray (Spraying Systems LLN-1/4 1.5), full-cone spray (ISR prototype nozzle), and a flat fan spray (Spraying Systems H1/4VV). Photographs of the sprays produced by the three nozzles are shown on Fig. 2. Data were obtained at nozzle pressures between 207 kPa (30 psi) and 689 kPa (100 psi) and nozzle-to-surface distances between 3.0 mm and 7.0 mm.

A laser droplet size analyzer (Malvern) was used to estimate the droplet size distribution. Individual droplets in the spray scattered the light from a red laser 10 mm in diameter. The collector consisted of a number of concentric photodetectors which measured the light intensity. Smaller droplets resulted in more light striking the detectors further from the center, enabling the fraction of droplets within a certain diameter range to be determined.

The spray was placed in an airtight Plexiglas chamber and the working fluid was circulated in the chamber via a pump (Cole Palmer, 75211-10). For each nozzle, droplet size measurements were carried out for pressures ranging from 138–896 kPa (20–130 psi) with the axis of the laser positioned 8 mm and 10 mm below the spray nozzle orifice. Misalignment between the source and the collector, scattering from the chamber walls, ambient light, and mist could cause significant background noise. Therefore, in addition to compensating for sources of error in the system each test was performed twice to ensure repeatability of the results and averaged. One of the largest sources of error occured when the deflected laser was scattered multiple times by different spray drops, resulting in artificially small droplets. The full-cone spray could not be tested as a result. Mist was another source of error. Since liquid was sprayed into a relatively small chamber, mist formed due to drops rebounding off surfaces within the chamber. To correct for the background mist, the spray was suddenly cut off at each pressure and droplet size measurements were immediately obtained before the mist could settle. These measurements took into account the effects of ambient light, background noise, and mist, and were subtracted from the measurements with spray. d_{32} for the full-cone spray was estimated from the correlation of Estes and Mudawar (1995)

$$\frac{d_{32}}{d_0} = 3.07\left(\frac{\rho_v^{1/2}\Delta P d_0^{3/2}}{\sigma^{1/2}\mu_l}\right)^{-0.259} \tag{9}$$

to be 40–65 μm over the range of pressures tested. The mean absolute error of this correlation is claimed to be 12%.

The flow rate through the spray nozzles in Table 1 were determined by measuring the time required to collect 50 ml of liquid in a graduated cylinder. The droplet velocities were estimated from Ghodbane and Holman (1991):

$$V_0 = \left[V_{tube}^2 + \frac{2\Delta P}{\rho} - \frac{12\sigma}{\rho d_{32}}\right]^{1/2} \tag{10}$$

A summary of the spray conditions and characteristics is given in Table 1. The droplet size remains fairly constant for the hollow cone and flat fan spray, but the droplet velocity changes by a factor of two.

Fig. 2. Photographs of sprays produced by three nozzle types operating at 344 kPa.

2.2. Pressure measurement apparatus

A schematic of the test rig used to measure the pressure distribution is shown on Fig. 3. The local pressure was measured using a pressure transducer connected to a 3.2 mm (0.125 in.) diameter hole drilled halfway through a plexiglass plate. Proper design of the pressure tap was important to obtaining accurate pressure readings for the low pressures being measured. The pressure tap was formed by machining a 0.1 mm diameter hole into the plate. Since any liquid in the tap decreases the measured pressure reading in a gravity field due to its head, the height of liquid within the tap was minimized by drilling a 4 mm diameter hole into the pressure plate perpendicular to the tap resulting in a tap length of 5.0 mm. The largest pressure reduction this would cause in the measured pressure for the fluid used (PF-5060) can be calculated to be 49 Pa, which is smaller than the uncertainty in the pressure measurement and much smaller than the pressures produced by the sprays in this study. Any liquid that did enter the tap drained into a 30 ml flask that served as a liquid trap. The trap could be drained periodically using a solenoid valve. The pressure transducer used for the hollow and full-cone spray data was a differential pressure gauge with range of 0–5.0 kPa (All Sensors Model 20 INCH-D-4V), while the transducer for the flat spray had a range of ± 34.5 kPa (All Sensors Model 5 PSI-D-4V).

Two orthogonal motorized translation stages (Zaber T-LS13-M, 13 mm travel with 0.1 μm positioning resolution) were used to traverse the pressure tap in the two directions perpendicular to the spray axis in 350 μm steps in the form of a 32 × 32 matrix. The translation stages were always driven in the same direction to eliminate positioning errors due to backlash. A precision-machined spacer block was used to set the distance between the spray nozzle and the pressure tap. After each step, a time delay was provided to allow the pressure to stabilize before data were acquired. The proper time delay for each case was determined by increasing the time delay until no changes in pressure were observed. Delays of 5 s were required for the pressures between 207 kPa and 344 kPa, and a delay of 10 s was required for higher pressures. The spray was oriented upward such that any excess liquid fell off the Plexiglas plate to minimize erroneous readings due to any buildup of stagnant liquid on the surface. The pressure distribution was measured in 0.35 mm increments. The output of the pressure transducer was sampled using a 12 bit A/D converter.

Table 1
Summary of flow and spray characteristics.

Nozzle	Pressure (kPa)	Flow rate (m/s)	Laser distance (mm)	d_{32} (μm)	Droplet velocity (m/s)
Hollow cone	207	1.04	8	27	15.7
	344	1.28	8	27	20.2
	483	1.56	8	28	23.9
	689	1.72	8	28	28.6
	896	2.00	8	25	32.6
	207	1.04	10	24	15.7
	344	1.28	10	24	20.2
	483	1.56	10	25	23.9
	689	1.72	10	25	28.6
	896	2.00	10	25	32.6
Flat fan	207	2.17	8	30	15.7
	344	2.63	8	27	20.2
	483	2.94	8	23	23.9
	689	3.33	8	19	28.6
	896	3.85	8	16	32.6
	207	2.17	10	31	15.7
	344	2.63	10	26	20.2
	483	2.94	10	21	23.9
	689	3.33	10	17	28.6
	896	3.85	10	15	32.6
Full cone	138	2.22	N/A	65[a]	12.8
	207	2.79	N/A	58[a]	15.7
	344	3.57	N/A	51[a]	20.2
	483	4.30	N/A	47[a]	23.9
	689	5.43	N/A	43[a]	28.6
	896	6.25	N/A	40[a]	32.6

[a] Data obtained from Eq. (9).

2.3. Heat transfer coefficient measurement apparatus

2.3.1. Microheater array

An array of 96 microheaters was used to obtain measurements of the spatial heat transfer distribution on the surface (Fig. 4). Each heater element was nominally 700 μm in size and consisted of a thin (200 nm thick, 7 μm wide) serpentine platinum resistance heater and a titanium adhesion layer sputtered onto a 500 μm thick quartz substrate. Thicker gold leads were deposited up to the edge of the array to ensure minimal lead resistance (<1 Ω), and the entire array was covered with a 1 μm SiO_2 passivation layer to provide a uniform surface energy. The individual heater elements were maintained at a uniform specified temperature using 96 Wheatstone bridge feedback circuits. The temperature of each element was selected through the use of a 20 kΩ digital potentiometer with 512 discrete steps. When combined with the other resistor elements in the circuit, the array temperature could be set from 30 °C to 110 °C with a resolution of approximately 0.2 °C. The frequency response of the combined heater/bridge circuit was approximately 15 kHz. Each heater was capable of dissipating 2.0 W, or a maximum surface heat flux of 400 W/cm^2. Additional details regarding the working principles of the microheater array are available in Rule and Kim (1999) and Bae et al. (1999). The heaters on the edge of the array serve as guard heaters to minimize heat leakage through the substrate. Data from only the middle 64 heaters were used in this study.

2.3.2. Test chamber

PF-5060 was pumped from the fluid reservoir through a positive displacement pump, a filter, then through the spray nozzles. The atomized liquid impacted the heater array located at the bottom of the spray chamber. Excess liquid and condensed vapor could drain from the spray chamber back to the fluid reservoir by gravity. The standoff distance between the heater and the spray could be adjusted using a set of three orthogonal traverses with accuracy of 25.4 μm (0.001 in.). A camera mounted on a tripod head and fixture below the chamber allowed the spray axis to be adjusted over the center of the heater with an accuracy of approximately 0.2 mm. A thermocouple placed before the nozzle monitored the liquid temperature to assure constant temperature throughout the data acquisition time.

The spray nozzle could be moved within the spray chamber using a set of three orthogonal traverses. In the case of the hollow cone spray for stand-off distances of 5 mm and 7 mm, the spray impact region was larger than the heater size. To acquire data for the entire region, the spray was positioned over the four corners of the middle 8 × 8 heaters and the heat transfer data for a quarter of the spray was collected. The data sets were subsequently merged to create the full heat transfer distribution pattern in form of a 16 × 16 matrix.

2.4. Test conditions

Pressure and heat transfer coefficient distributions were obtained at all combinations of nozzle types (hollow cone, full cone, and flat spray), operating pressures (207 kPa, 344 kPa, 483 kPa, and 689 kPa), and stand-off distances (3.0 mm, 5.0 mm, and

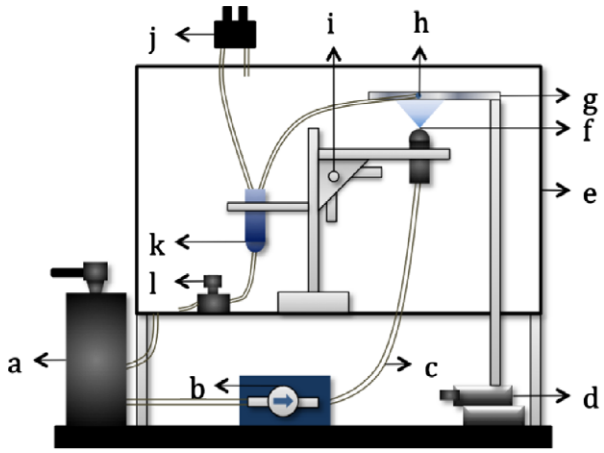

a	Fluid reservoir
b	Pump
c	Fluid line
d	Motor driven micrometer stage (2 directions)
e	Plexglas chamber
f	Spray nozzle
g	Pressure plate
h	Liquid drain
i	Nozzle support
j	Pressure transudcer
k	Liquid trap
l	Solenoid valve

(a) Overall schematic

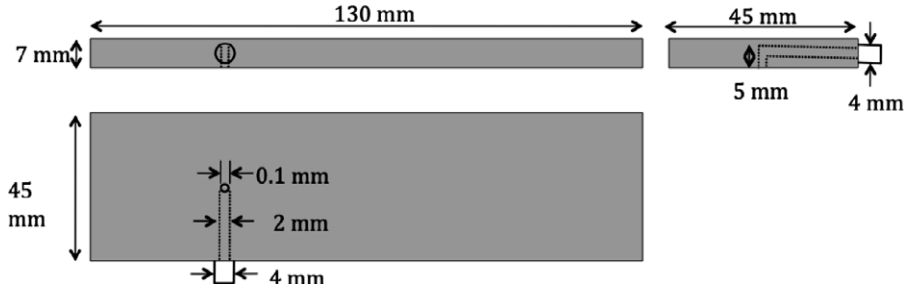

(b) Details of pressure tap in pressure plate.

Fig. 3. Schematic of pressure measurement apparatus showing detail of pressure tap geometry in the pressure plate.

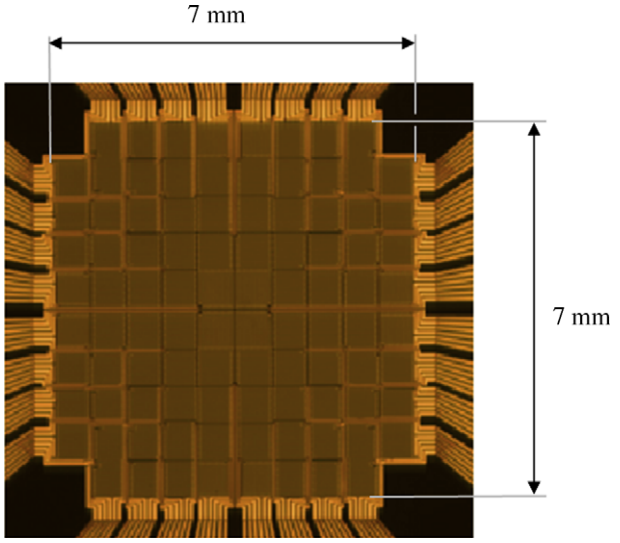

Fig. 4. Photograph of microheater array used to measure heat transfer coefficient distribution.

7.0 mm). Heat transfer data were obtained at heater temperatures between 40 and 90 °C in 5 °C increments. Since the saturation temperature of PF-5060 was 56 °C, only heat transfer data for temperatures between 40 °C and 60 °C were used to calculate the heat transfer coefficient.

2.5. Data reduction and uncertainty analysis

2.5.1. Pressure measurement

Both of the pressure transducers used to collect data had a nominal linearity and hysteresis error of ±0.5% of their full scale which corresponded to uncertainties of ±25 and ±172 Pa for smaller and larger transducers respectively. The other major sources of uncertainty in the pressure measurement apparatus was due the pressure tap length which created a reverse head and caused up to 49.4 Pa pressure reduction in the measurements. The uncertainty in standoff distance was approximately one mark on the orthogonal traverse set (±25 μm).

Because the pressure was sampled over a $11.2 \times 11.2\ mm^2$ area at twice the resolution of the heater array, two steps were performed so a correlation between pressure and heat transfer could be obtained. First, a 16×16 pixel subset of the original pressure data was chosen by eye such that the location of the peaks in the pressure distribution and the peaks in the h distribution matched. This pressure data were then "coarsened" into 8×8 squares each composed of 2×2 pixels, and the pressure was averaged within each square to obtain an 8×8 array of averaged pressure that corresponded to the heat transfer data.

2.5.2. Heat transfer coefficient measurement

The heat transfer coefficient was determined from

$$h = \frac{\dot{q}''}{T_{surface} - T_{spray}} \tag{11}$$

where $T_{surface}$ and T_{spray} were the temperatures of the microheater array and spray, respectively. The spray temperature was controlled to be 30 °C for all cases. The heat flux data obtained with the microheater array set at 60 °C were chosen to compute the h distribution since this was the highest temperature at which data were taken within the single-phase regime, thereby minimizing the uncertainty in h.

The uncertainty in heat flux has been discussed in previous work by Horacek et al. (2005), and will not be repeated here. In summary, the uncertainty in the heat flux due to measurement errors resulted from uncertainties in the heat supplied to the heaters and the heat conducted into the substrate by conduction. The final uncertainty in heat transfer due to measurement inaccuracies in the feedback circuit and data acquisition system was conservatively calculated to be less than 3%. Larger uncertainties in the spray cooling curve could result from uncertainties in liquid flow rate, wall temperature, and dissolved gas concentration. The liquid flow rate was steady to within 0.5 ml/min (1.4–4.5% over the range of flow rates tested). The uncertainty in wall temperature was assumed to be two positions on the digital potentiometer, or 0.4 °C. The amount of gas in the flow loop was determined by measuring the pressure and temperature in the flow loop. The distribution of the gas, however, could vary within the flow loop if the temperatures varied (which is likely since the heater was hotter than the surroundings), making it difficult to quantify the local gas concentration. Repeated measurements of the spray cooling curves under the same nominal conditions resulted in errors of about 4%. The total uncertainty in the spray cooling curves obtained by combining the uncertainty in repeatability with the measurement inaccuracies was estimated to be 5%.

It should also be noted that there were numerous non-operational heaters in the array (the heater resistances were abnormally low or high so their control circuits were disabled), and another few that were occasionally non-regulating (the heaters did not respond to variations in heat flux). The total number and location of the non-regulating heaters varied from case-to-case, with the number of non-regulating heaters typically decreasing with increasing heater temperature. Additional non-regulating heaters were observed in the low heat flux regions away from the spray

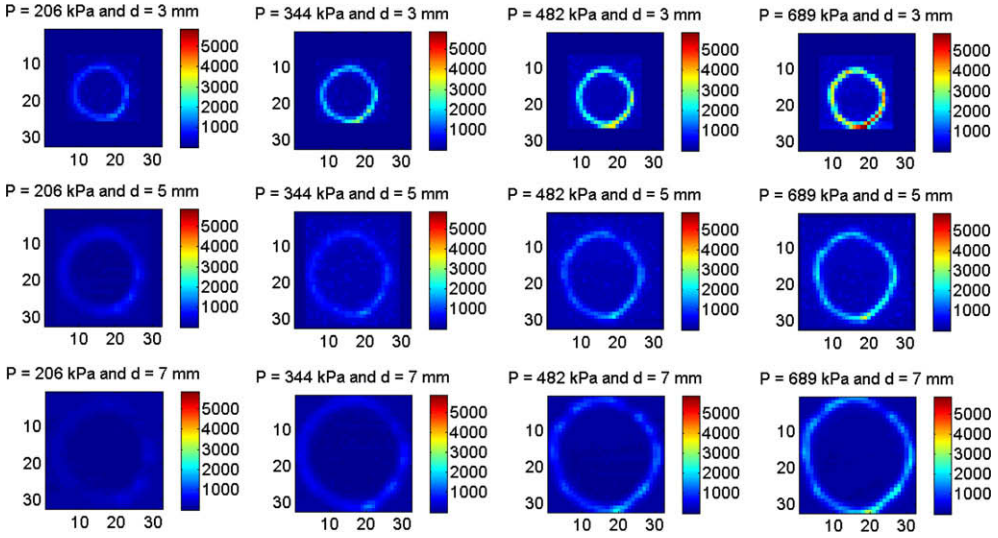

Fig. 5. Impingement pressure distribution for hollow cone sprays.

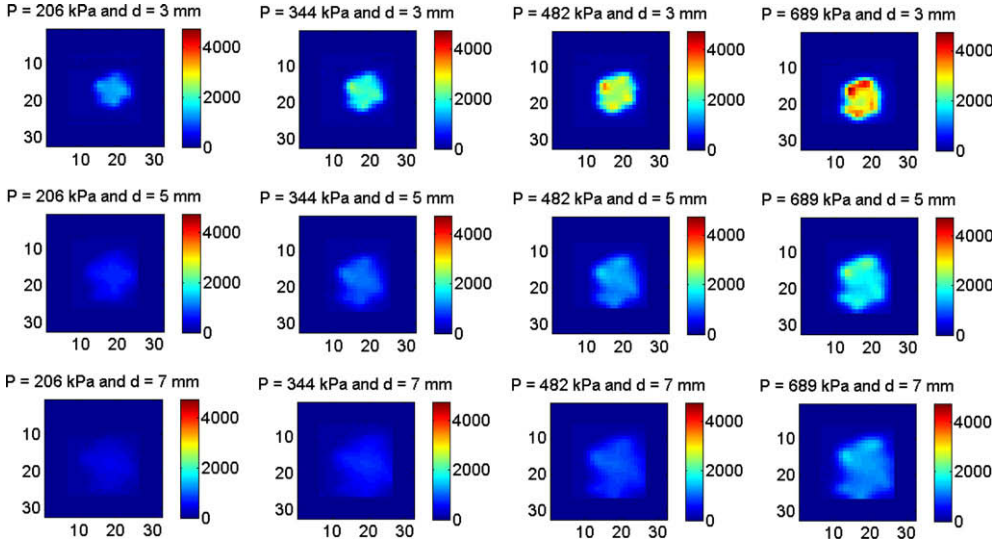

Fig. 6. Impingement pressure distribution for full-cone sprays.

impact region. The reasons the non-regulating heaters occur are not completely understood at this time, but may be due to thermal interactions between adjacent heaters. The heaters adjacent to these non-operational and non-regulating heaters were observed to dissipate abnormally high heat transfer since they partially compensate for lack of heat from the non-operational heaters. For this reason, the non-regulating heaters as well as their immediate neighbors were excluded in the heat transfer study.

3. Results and discussion

3.1. Pressure and heat transfer measurements

The pressure distribution produced by the three spray nozzles at all nozzle pressures and stand-off distances are shown in Figs. 5–7. It is observed that as the nozzle-to-plate spacing increases, the overall pressure decreases but the area experiencing elevated pressure increases. The diameter of the elevated pressure region is relatively constant with nozzle pressure for the hollow and full-cone sprays. The pressure distributions produced by the hollow cone and full-cone sprays are not radially symmetric as one might expect, and are likely due to imperfections in the spray nozzle or asymmetries in the liquid inlet velocity. The linear spray produces significantly higher peak pressures than the other two (over 20 kPa) since the flow rate is higher for a given nozzle pressure difference (Table 1) and the spray is concentrated within a narrow band, resulting in more droplets striking the surface with a higher velocity.

The heat transfer coefficient data shown on Figs. 8–10 shows similar trends. The effect of non-regulating and non-functional heaters on the heat transfer distribution is evident from the drop-outs in the data (dark colored heaters). The regions of elevated heat transfer correspond well with the regions of elevated pressure (the pressure data in Figs. 5–7 have twice the spatial resolution as the heat transfer data).

In order to minimize the effect of noise in both the pressure and heat transfer data so they could be compared, the local distributions produced by the hollow and full-cone sprays were radially

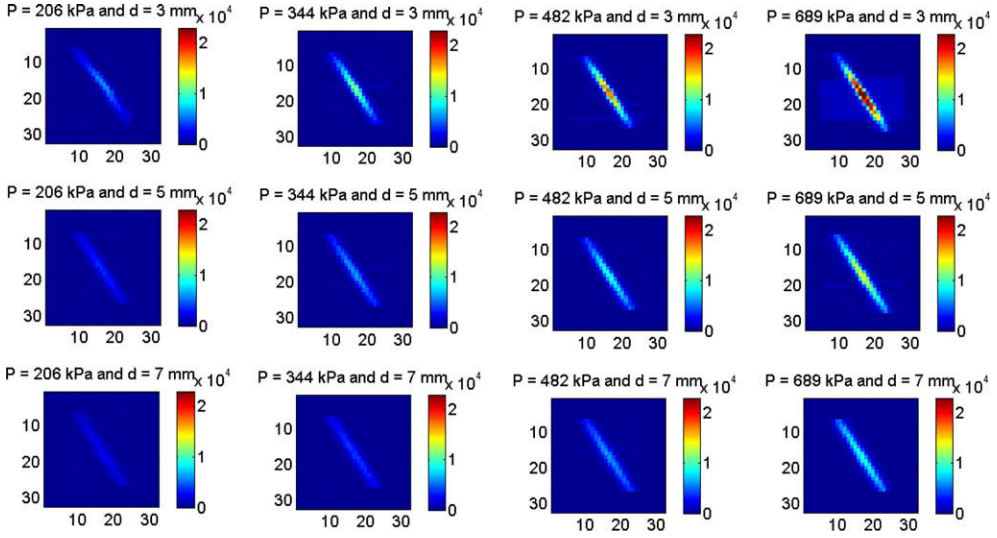

Fig. 7. Impingement pressure distribution for flat sprays.

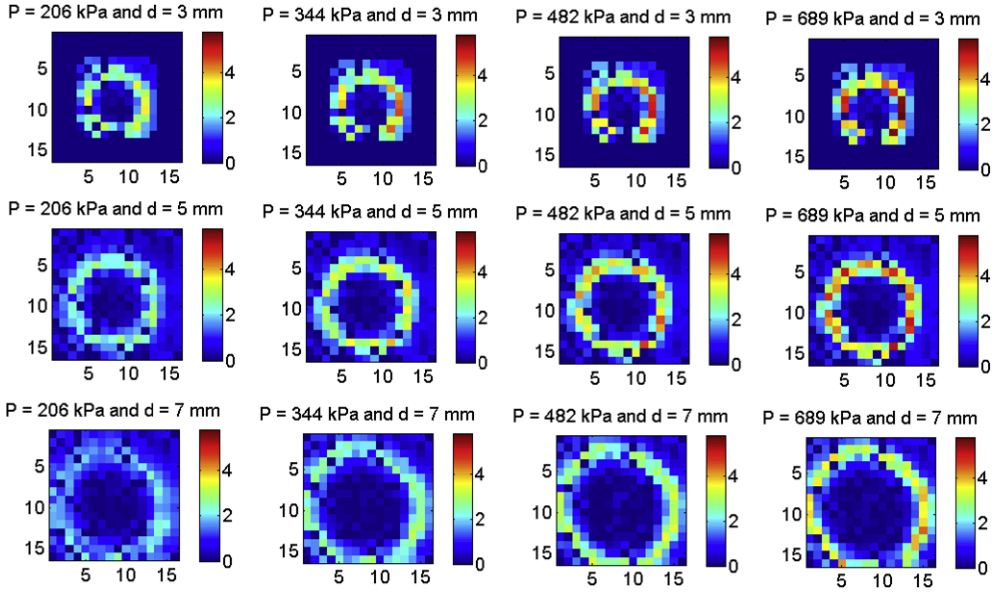

Fig. 8. Local heat transfer coefficient for hollow cone sprays.

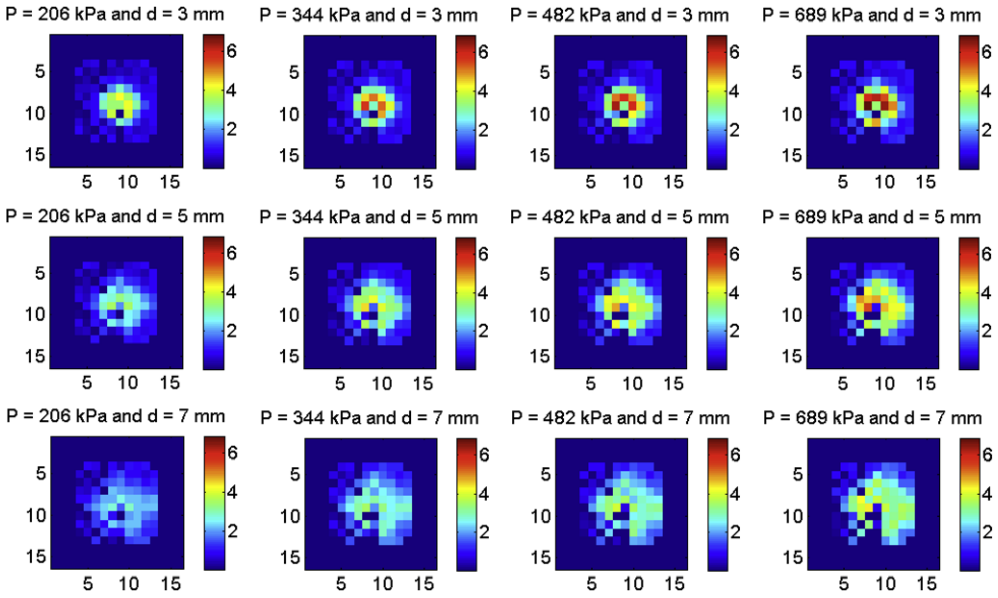

Fig. 9. Local heat transfer coefficient for full-cone sprays.

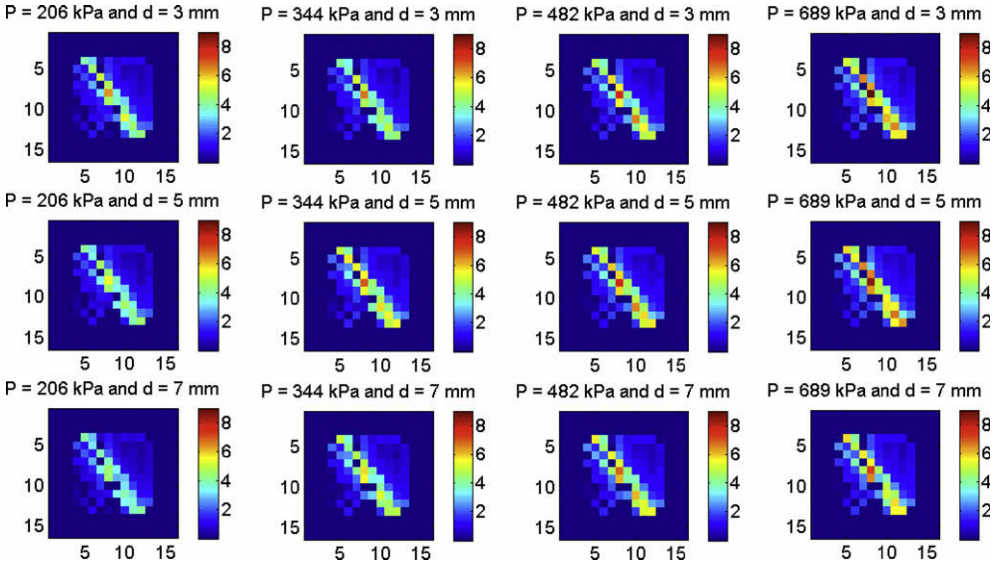

Fig. 10. Local heat transfer coefficient for flat sprays.

averaged. The center of the heater closest to the center of the spray cone was chosen to be the origin (x_0, y_0). The radial distance to the other heaters were then calculated as the distance between their centers from the origin. The averaged pressure and heat transfer distributions vs. radial location for the hollow cone and full-cone sprays are shown in Figs. 11 and 12. The location of the peaks in the pressure and heat transfer data occur at the same radial location for both nozzles, and the width of the pressure and heat transfer peaks are similar, consistent with our hypothesis. The magnitudes of the peaks increase with increasing pressure and decreasing standoff distance, as expected.

3.2. Correlation between and pressure and heat transfer coefficient

To obtain the correlation between pressure and heat transfer coefficient, the raw heat transfer coefficient data were binned and the values in each bin were averaged to obtain a single value for the heat transfer coefficients between P and $P + \Delta P$. This allows for proper weighting of the available data. For example, if many data points are available at a low pressure and only a few points are available at a higher pressure, the low pressure data would be disproportionately weighted when performing a least squares fit to the data. Binning allows equal weight to be given to data over the entire range of pressures irrespective of the number of data points obtained at any given pressure. It also has the added benefit of reducing noise in the data. The binned heat transfer vs. pressure data for the three nozzles are shown on Fig. 13 for a bin width $\Delta P = 100$ Pa. The heat transfer coefficients for the three nozzle types agree well with each other, lending strong support to the hypothesis.

Since the pressure and heat transfer were expected to have a correlation of the form $h = C_1 P^{1/2}$, a least squares fit was used to find the best fit for the constant C_1 when the data were restricted to 0–5000 Pa. This pressure range encompasses the entire data set for the hollow and full-cone sprays, but only part of the data for the flat fan spray. The results summarized on Table 2 indicate that the values of C_1 for the three nozzles agree closely, indicating that a single equation can be used for all nozzle types with reasonable

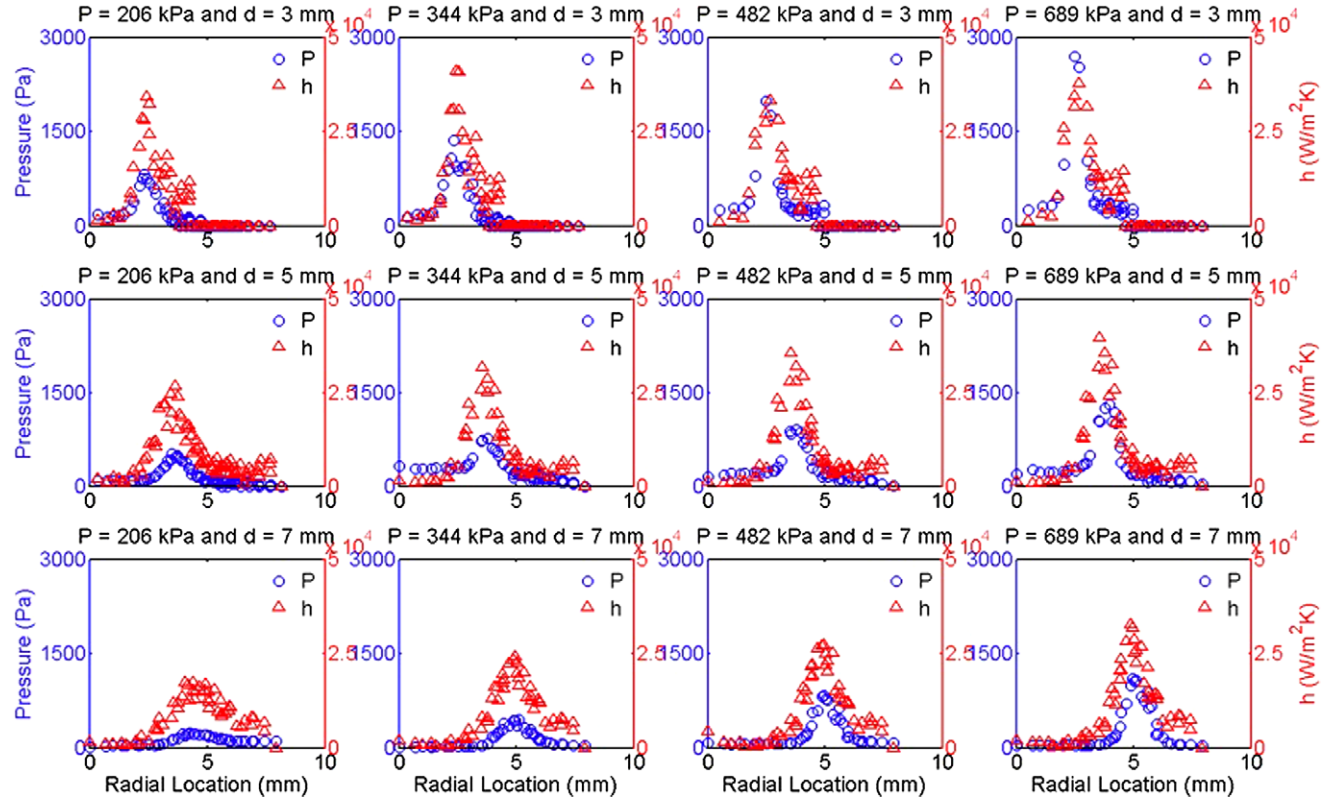

Fig. 11. Radial distributions of pressure and heat transfer coefficient for the hollow cone nozzle.

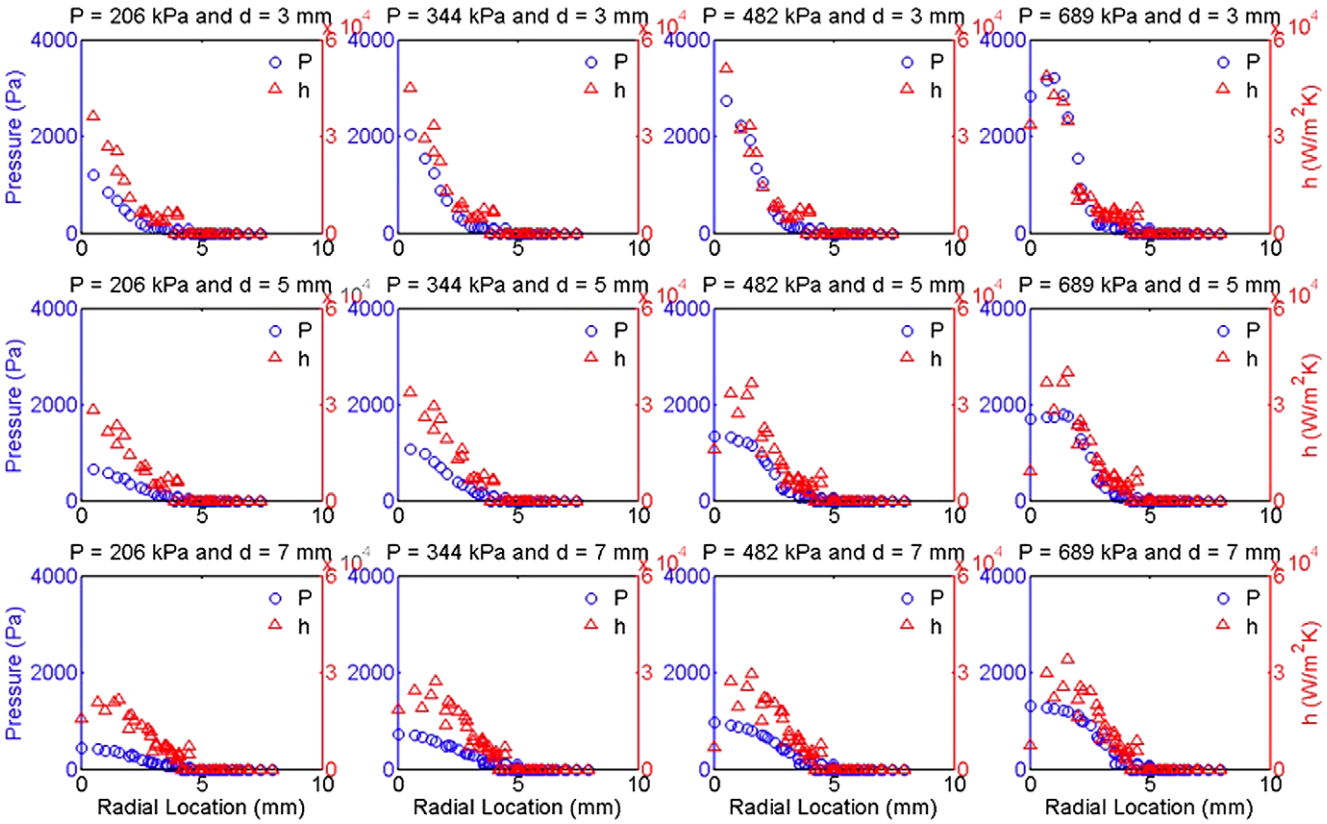

Fig. 12. Radial distribution of pressure and heat transfer coefficient for the full cone nozzle.

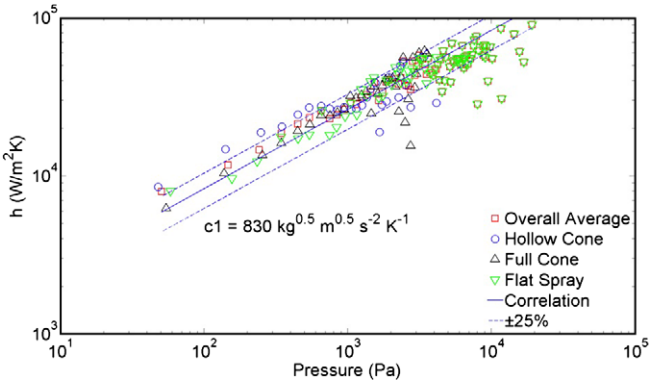

Fig. 13. Heat transfer vs. pressure data for the three nozzle types along with the average. The data was binned using $\Delta P = 100$ Pa.

Table 2
Summary of correlation data.

Spray nozzle	$C_1\left[\frac{kg^{1/2}-m^{1/2}}{s^2-K}\right]$	Pressure range (kPa)
Hollow cone	830	0–5000
Full cone	850	0–5000
Flat fan	810	0–5000
Flat fan	710	0–20,000

accuracy. The value of C_1 was found to be insensitive to bin widths between $\Delta P = 25$ Pa to $\Delta P = 100$ Pa. A correlation assuming $C_1 = 830\ \frac{kg^{1/2}m^{1/2}}{s^2K}$ is shown on Fig. 13 and agrees well with the data. The flat fan spray data for pressures above 5000 Pa are observed to fall somewhat below the correlation indicating that the higher pressure data may require a separate correlation, or another correlation with less accuracy will be needed if a single correlation is desired for the extended pressure range. A fit to the flat fan data alone (0–20,000 Pa) yielded $C_1 = 710\ \frac{kg^{1/2}m^{1/2}}{s^2K}$. Additional data using the hollow cone and full-cone sprays to produce local pressures higher than 5000 Pa should be obtained and combined with the flat fan data to extend the correlation to higher pressures.

This correlation can now be used to "predict" the local heat transfer coefficient from the measured pressure distribution. Comparison between the radially averaged, measured heat transfer coefficients and those obtained from the correlation for the hollow cone spray are shown on Fig. 14. In some cases, the heat transfer in the droplet impact region is underpredicted while the heat transfer in the low pressure region is overpredicted, but the correlation predicts the data reasonably well. The full-cone spray data (Fig. 15) is predicted very well by the correlation.

Comparison between the measured and predicted area averaged heat transfer over the entire heated area is shown on Fig. 16. The local pressure was used to calculate a local heat transfer coefficient, which was then averaged over all heaters in the array. Agreement to within 25% is observed for almost all of the data.

4. Conclusions

The work described in this paper has provided strong evidence that the local spray cooling heat transfer coefficient can be correlated remarkably well with the local pressure in the single-phase heat transfer regime. The correlation developed here for PF-5060 is applicable when the normal pressures are below 5000 Pa. The correlation will be validated in future work using other fluids, with

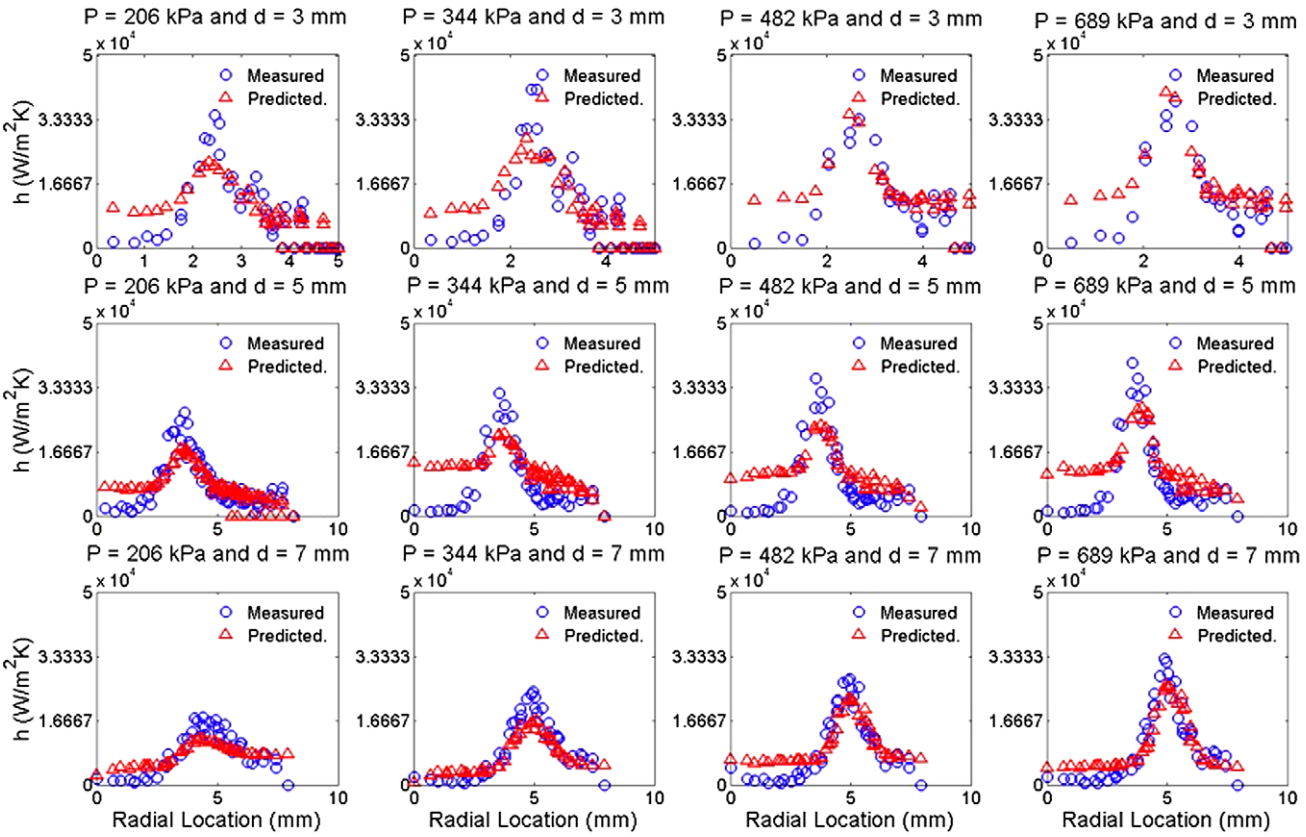

Fig. 14. Comparison of the measured heat transfer coefficients with the correlation, hollow cone sprays.

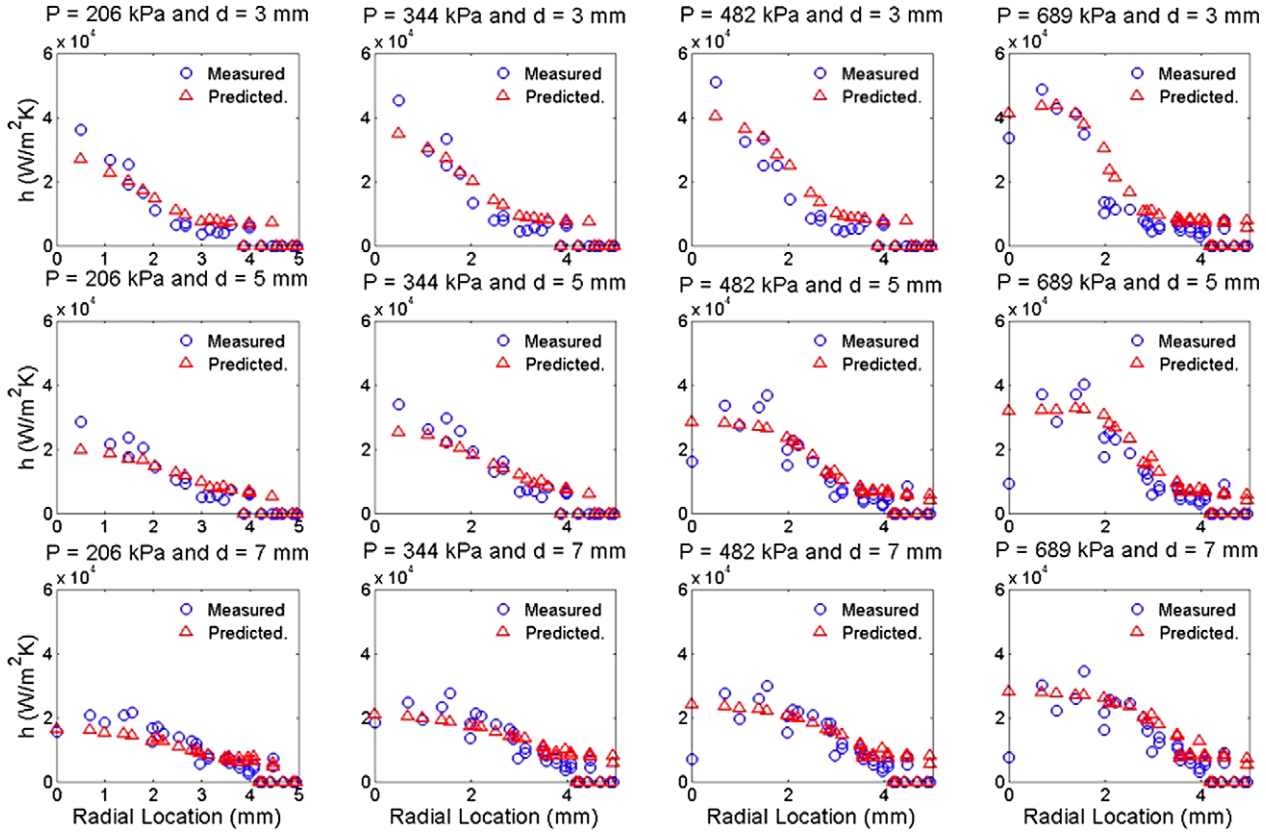

Fig. 15. Comparison of the measured heat transfer coefficients with the correlation, full cone sprays.

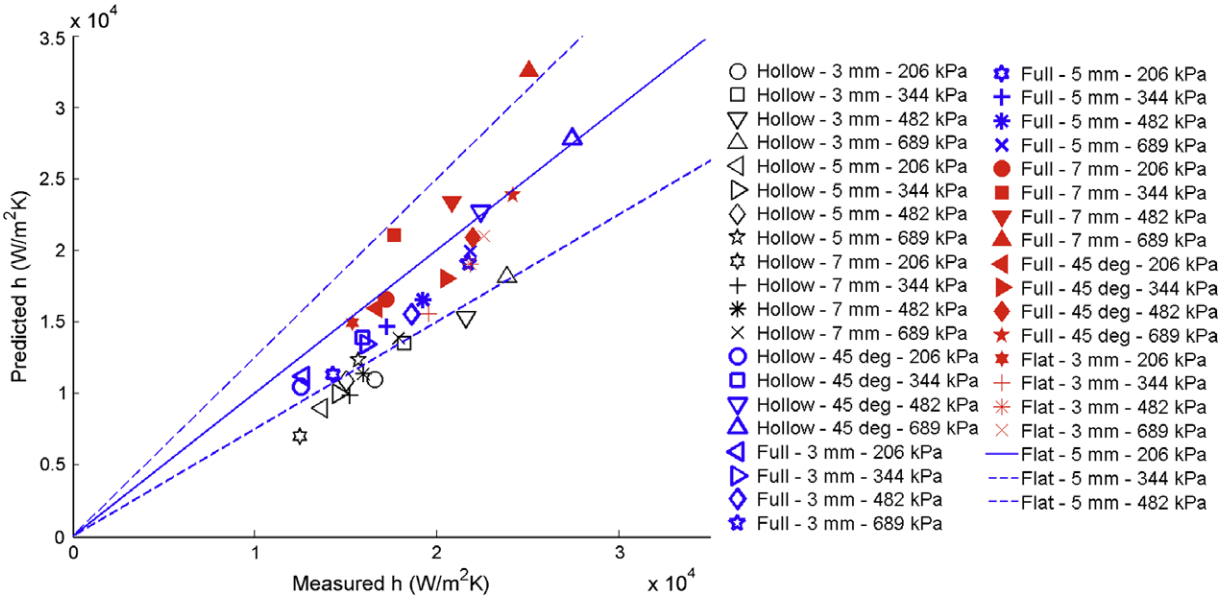

Fig. 16. Comparison between the measured area averaged heat transfer over the entire heated area with the heat transfer obtained from the pressure data and the correlation.

the nozzles oriented off-normal to the heater surface, and with multiple, overlapping nozzles.

Acknowledgments

This work was supported by the Office of Naval Research (Dr. Mark Spector) on Grant No. N000140711101.

References

Bae, S., Kim, M.H., Kim, J., 1999. Improved technique to measure time and space resolved heat transfer under single bubbles during saturated pool boiling of FC-72. Exp. Heat Transfer 12, 265–278.

Chen, J.C., 1966. Correlation for boiling heat transfer to saturated fluids in convective flow. Ind. Eng. Chem. Process Des. Develop. 5, 322–339.

Estes, K.A., Mudawar, I., 1995. Correlation of Sauter mean diameter and critical heat flux for spray cooling of small surfaces. Int. J. Heat Mass Transfer 38, 2985–2996.

Fedorchenko, A.I., Wang, A.B., 2004. On some common features of drop impact on liquid surfaces. Phys. Fluids 16, 1349–1365.
Ghodbane, M., Holman, J.P., 1991. Experimental study of spray cooling with Freon-113. Int. J. Heat Mass Transfer 34, 1163–1174.
Horacek, B., Kiger, K., Kim, J., 2005. Single nozzle spray cooling heat transfer mechanisms. Int. J. Heat Mass Transfer 48, 1425–1438.
Josserand, C., Zaleski, S., 2003. Droplet splashing on a thin film. Phys. Fluids 15, 1650–1657.
Kim, J., 2007. Spray cooling heat transfer: the state of the art. Int. J. Heat Fluid Flow 28, 753–767.
Pautsch, A.G., Shedd, T.A., 2006. Adiabatic and diabatic measurements of the liquid film thickness during spray cooling with FC-72. Int. J. Heat Mass Transfer 49, 2610–2618.
Prosperetti, A., Oguz, H.N., 1993. The impact of drops on liquid surfaces and the underwater noise of rain. Annu. Rev. Fluid Mech. 25, 577–602.
Rioboo, R., Tropea, C., Marengo, M., 2001. Outcomes from a drop impact on solid surfaces. Atomization Spray. 11, 155–165.
Rule, T.D., Kim, J., 1999. Heat transfer behavior on small horizontal heaters during pool boiling of FC-72. J. Heat Transfer 121, 386–393.
Rybicki, J.R., Mudawar, I., 2006. Single-phase and two phase cooling characteristics of upward-facing and downward facing sprays. Int. J. Heat Mass Transfer 29, 5–16.
Shedd, T.A., 2007. Next generation spray cooling: high heat flux management in compact spaces. Heat Transfer Eng. 28, 87–92.
Weiss, D., Yarin, A., 1999. Single drop impact onto liquid films: neck distortion, Jetting, tiny bubble entrainment, and crown formation. J. Fluid Mech. 385, 229–254.
Yarin, A.L., 2006. Drop impact dynamics: splashing spreading, receding, bouncing. Annu. Rev. Fluid Mech. 38, 159–192.
Zhu, Y., Oguz, H.N., Prosperetti, A., 2000. On the mechanism of air entrainment by liquid jets at a free surface. J. Fluid Mech. 404, 151–177.